

Kai Berger · Jeyarajan Thiyagalingam

Real-time Pedestrian Surveillance with Top View Cumulative Grids

Received: date / Revised: date

Abstract This manuscript presents an efficient approach to map pedestrian surveillance footage to an aerial view for global assessment of features. The analysis of the footages relies on low level computer vision and enable real-time surveillance. While we neglect object tracking, we introduce cumulative grids on top view scene flow visualization to highlight situations of interest in the footage. Our approach is tested on multiview footage both from RGB cameras and, for the first time in the field, on RGB-D-sensors.

1 Introduction

The security of public areas is a critical part for pluralistic society. While we enjoy the freedom to use public facilities ranging from bus stations to airports for personal purposes, we have to be aware that these places are also the most likely areas for an impending attack with a high death toll. Apart from terroristic attacks, burglary and beggary are also most likely occur there, because these places bear with a great amount of anonymity for the subjects using them. Therefore, authorities strive to increase security with public surveillance (CCTV). Apart from the psychological factor, the camera system also directly helps avoiding crimes by live streams which help monitoring officers to alert ambulance. Further, recorded footage might later help convict suspects once the charges have been pressed by victims. Human operation to CCTV monitoring however introduces the risks that crucial events are missed due to attention shifts or blind spots in the surveillance area. Furthermore, when the video footage is juxtaposed on monitors, it becomes a non-trivial task for the monitoring officer to build a

K. Berger
OerC Oxford
E-mail: kai.berger@oerc.ox.ac.uk

J. Thiyagalingam
OerC Oxford
E-mail: jeyarajan.thiyagalingam@oerc.ox.ac.uk



Fig. 1 Input footage from a calibrated viewpoint (left, middle) and simplified satellite map (right).

mental map from the image streams. A subject leaving the imaged area in one window might not appear afterwards in neighboring windows. To tackle this problem, several high-level computer vision algorithms have been proposed, to recognise, label and track subjects image by CCTV. However, a failure of such a system to detect a single subject once can become fatal, if that subject turns out to be the villain, or a terrorist. In this paper we want to overcome the weaknesses of both the juxtaposition of image streams for human-based monitoring and the high-level vision based automatic tracking. We propose to build the mental map virtually by rendering a top view from one to many input cameras. The evaluation of the depicted motion is left to the human monitoring officer but our algorithm visualizes occupancy times and the scene flow on the top view to help with the judgement of a given situation. For the first time, we present an approach that incorporates traditional RGB camera based scene surveillance and depth-value based scene surveillances, e.g. from RGB-D sensors or Time-Of-Flight cameras. This enables new hardware setups for public areas, based on depth-sensors that have increasingly gotten affordable over the last three years and that help surveying scenes with varying lighting conditions.

The paper is structured as follows: after briefly reviewing the state of the art in Sect. 2, we will present an approach to retarget pedestrian surveillance footage into the topview in order to perform motion and video analysis to it, Sect. 3. Two algorithms, one for RGB-data and one for depth data will be described in detail. The motion analysis consists of cumulative maps to help crowding detection and the application of optical flows.

In Sect. 4, we will apply the algorithm to an RGB outdoor dataset consisting of eight calibrated cameras and two indoor datasets, before we conclude in Sect. 5. One dataset is a depth-based dataset consisting of one ToF-camera, the other is the surveillance of a train station with for extrinsically calibrated RGB cameras.

2 Related Work

Reprojection and summarization

Image reprojection aims to warp an input image into an arbitrary viewpoint and a typical implementation using an energy functional minimization is formulated by Setlur *et al.*[41]. Carroll *et al.* [8] reprojects images in order to artistically introduce a new perspective to a given image, while Sacht *et al.* [39] reprojects photographic images into specific cylindrical views. The term *summarization* was coined by Daniel and Chen [11] to reproject an image sequence meaningfully into one single image and the was later refined by Botchen *et al.*[6]. Based on this approach it was shown [9] that ordinary users can learn to detect and recognise *visual signatures* of events from video visualization. Wang *et al.* [46] proposed to reproject videos into a 3D environment model for scene awareness. Legg *et al.* used homographic projection for 3D reconstruction from a single viewpoint [25] and Parry *et al.* applied this approach to image sequences in sports [33]. Remero *et al.* [37] summarized activities captured by an aerial camera in natural settings. Further information can be found in a comprehensive survey on video-based graphics and video visualization conducted by Borgo *et al.* [5].

Pedestrian Surveillance Classically computer vision strives to detect pedestrians in input footage rather than reprojecting them meaningfully. For example Bayesian classifiers [49] to evaluate the presence of an object are widely employed for detecting pedestrians [12, 13]. Multi-person tracking has been implemented differently: the authors of [42] track pedestrians by flow optimization on the ground plane. The authors expand the algorithm with global appearance rules. The method proposed in [3] labels pedestrians the problem by estimating both discrete data and continuous trajectories using global costs. This method relies solely on trajectories and does not involve appearance of. Generally, association between data can be performed over a list of frames [34], e.g. in a hierarchical manner. In [22] the authors use tracklets from lower levels in the pyramid and associate them accordingly at a higher level to reduce the computational load. This method introduced in [22] is hierarchical, for example, and uses existing low-level tracklets. In [17], the tracks of pedestrians are refined with motion models. Multi-view methods have been introduced to overcome occlusion introduced in crowding scenarios. Currently, some multi-view based papers [47, 32] learn context models. Crowd density estimations can be used [38]

to improve human detection and tracking. The authors of [32] propose an adaptation scheme in which classifiers are learned incrementally through online boosting, so that they adapt to the changes over time. In [44], the authors propose to match a bipartite graph.

RGB-D Imaging Shotton *et al.* [43] introduced the Kinect and its underlying algorithm as a tool to capture the human pose from monocular depth images and paved the road for consumer-grade motion capturing with the device. In the wake of the commercial success monocular motion capturing has become the focus of the research community [16, 36, 30]. Mainly, the Microsoft Kinect was used capture datasets and benchmarks. Besides the tracking of limbs and joints quickly other research fields in monocular depth processing have emerged.

One research direction for example was to use the Microsoft Kinect as a hand-tracking device [31]. Frati *et al.* [15] assume the hand to always be closest limb to the camera while Reheja and his colleagues detect the palm with a circular filter the depth image [35]. Van den Bergh *et al.* [45] estimate the orientation of the hand from the orientation of the forearm in the depth image. Zollhofer *et al.* [50] fitted deformable facial meshes to depth data captured from human faces by relying on feature points (eyes, nose) in the depth data. Leyvand *et al.* also examine the face recognition of identical twins given depth and motion data from the Microsoft Kinect [26].

In 2011, Berger and his colleagues showed, that it is also possible to employ multiple depth sensors in one scene for motion capturing research [4]. Using an external hardware shutter [40] they were able to reduce the sensor noise introduced from neighboring Kinects. A similar approach has been introduced by Maimone and Fuchs [28]: each Kinect sensor shakes around its up vector introducing scene motion. This approach was refined by Butler *et al.* [7] who introduce arbitrary motion to the sensor which has to hang in an acrylic frame and has to be held by rubber bands.

Beside the Kinect sensor, depth imaging is usually conducted by passive stereo or with Time of Flight imaging. Most methods use the range imaging data to initialize stereo matching and impose constraints on the search range depending on the range imaging and stereo noise model. Local methods [24, 18, 20, 10, 48, 29] combine the stereo and the range imaging data term on a per pixel level. Kuhnert *et al.* and Hahne *et al.* [24, 20] compute confidences in the depth image and let stereo refine the result in regions with low confidence. Nair *et al.* [29] and Dal Mutto *et al.* [10] combine confidences from both stereo and the depth image into a stereo matching framework. Global methods such as [14, 19, 23, 29] use spatial regularization techniques in order to propagate more information to regions with low stereo or depth image confidence. Among the global methods, Fischer *et al.* [14] apply an extension of half global matching [21] to additionally handle depth data. Hahne *et al.* [19] applied a graph cut approach with a discrete number of disparities



Fig. 2 A pedestrian captured by two cameras (first, second) is mapped to a top-view by finding edge segments colinear with the mean optical flow vector of the pedestrian in each camera image (third, fourth). Corresponding areas in between the edge segments are intersected (fifth) to get the overlay in the aerial view (sixth).

to sensor fusion. Kim et al. [23] and Nair et. al [29] formulate the fusion problem in as a energy functional that is then minimized. Nair et al.[29] employ adaptive first and second order total variation (TV) with L1 regularization. normally used to estimate optical flow.

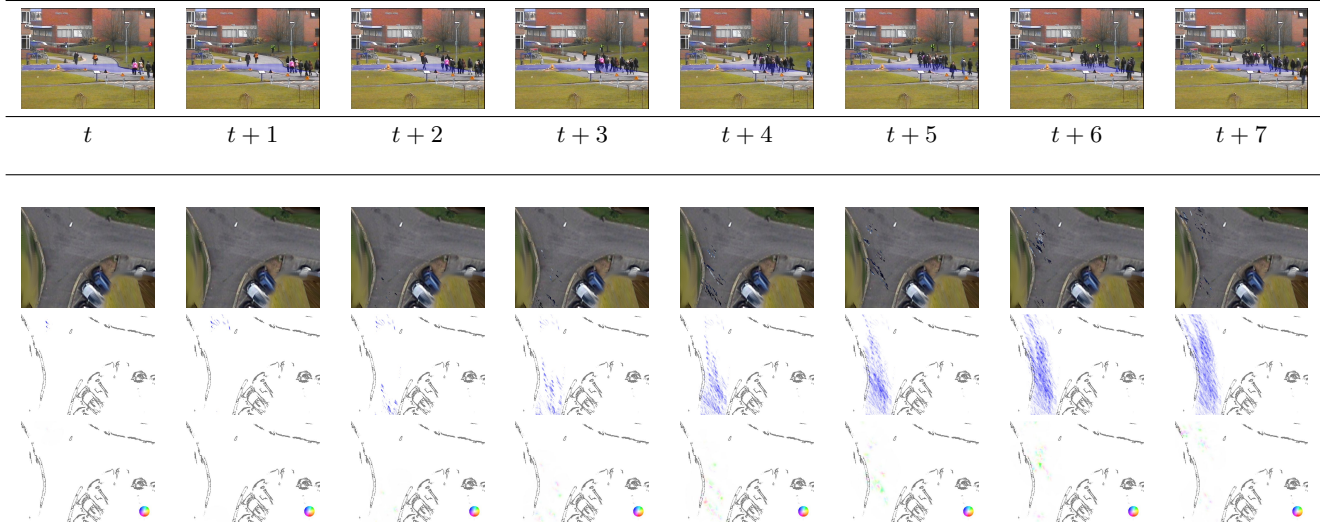
3 Proposed Algorithm and Test Datasets

In this section we describe the algorithm for top view summarization maps in detail. Its key idea is outlined in Fig. 2. For each input view $v \in V_{in}$ the algorithm, Alg. 1, requires a background image $I_{v,bg}$ and two consecutive images $I_{v,t}, I_{v,t-1}$. A background image can either be manually set by the user ($I_{v,bg} = I_{v,t_{user}}$) or aquired as mean intensity image over a time span T ($I_{v,bg} = \frac{\sum_t I_{v,t}}{T}$). In order to reproject pixel areas comprised by pedestrians into a topview with a calibrated Homography $W_v : v \in V_{in} \rightarrow v_{topview} \in V_{target}$ the algorithm searches for regions near edges that move parallel to the mean direction of motion for each pedestrian. This can be reasoned by the fact, that in a head-and-shoulder view, i.e. a top view $v_{topview} \in V_{target}$, only head, should and feet are visible and these body parts mainly contribute to edges $e_{\parallel} \in I_{edge,v,t}$ in an edge image $\in I_{edge,v,t}$ that are parallel to the mean direction of motion $\mathbf{v}_{pedestrian}$ of a pedestrian in a corresponding flow image $I_{flow,v,t}$, while most other body parts appear perpendicular. Thus, the algorithm computes the edge image $I_{edge,v,t}$ of the latest frame and, using the previous frame, it computes the mean flow vector for each pedestrian, i.e. each connected component $CC_{v,t}$ using the optical flow evaluation $I_{flow,v,t}$. This is done by calling Alg. 2. The computation of connected components is performed using the background image $I_{v,bg}$ and a significant colour distance. After having retrieved the mean optical flow vector for each connected component, which is equal to the mean direction of motion for each pedestrian in the image, Alg. 1 calls Alg. 3, which thresholds each edge segment for its collinearity to the mean flow of each object respectively. The threshold is performed by computing the angular difference between the flow vector and the normal to the gradient at each edge pixel and thresholding for the angular difference. Pixel regions in between the remaining edge pixels are filled in a line-sweep manner to arrive at a subset of the con-

nected component pixels. Using the camera calibration, Alg. 1 retargets the remaining pixels into the top view. To avoid distortions that linearly increase with distance form the ground plane, the algorithm intersets the reprojected pixel sets from all viewpoints to arrive a the intersection set coinciding with the area actually comprised by the pedestrian in a hypothetical top view. In table 1 we show the outcome of Alg. 1 on the PETS 2007 database [2]. In that scenario cameras are installed on the campus located at 5126'18.5N 00056'40.00W to cover an approximate area of 100m x 30m. The frames from different views can be considered as synchronised, but there are slight delays and frame drops detectable on rare occasions. The footage was not colour-corrected afterwards. The calibration has been performed with visual marks and Tsai Camera Calibration. The ground plane is assumed to be the Z=0 plane. All spatial measurements have been conducted in metres. The recorded frames were compressed as JPEG image sequences. Different sequences depict random walking crowd flow and regular walking pace crowd flow of different sparsity and with varying lighting conditions ranging from overcast to bright sunshine. Further walking, running, evacuation, i.e., rapid dispersion, local dispersion, crowd formation and splitting at different time instances have been simulated by the actors. Note, that we apply the motion analysis to the sequence in the topview, by computing a cumulative grid, Table 1 third row, and the optical flow for each pixel set, Table 1 fourth row. The cumulative grid is implemented by applying a cumulative moving average $A_t = \frac{p_1(x,y) + \dots + p_t(x,y)}{t}$. We may constrict the time span of the cumulative grid to a reasonable value t_{span} , for example several minutes. The implementation may then be altered to arrive at the following formula $A_t = A_{t-1} - \frac{p_{t-t_{span}}(x,y)}{t_{span}} + \frac{p_t(x,y)}{t_{span}}$.

In order to make the algorithm applicable for depth-sensor data as well a few alterations are necessary. First, the edge detection is performed on a single channel image and the contrast is at contact borders (e.g., when a foot is rested on the ground), Fig. 4.. Second, the re-projection $W_v : v \in V_{in,depth} \rightarrow v_{topview} \in V_{target}$ to the topview can be implemented by exploiting the camera calibration and the depth values, which avoids distortion errors as described in the previous case. Thus, Alg. 4 is implemented to search for edges in the depth maps

Table 1 Analysis and summarization of a pedestrian database [2]. The crowding that is noticeable at time frames $t + 2, t + 3, t + 4$ in the input images (first row) can be directly read from the cumulative top view scatterplot (third row). An optical flow computation can be applied to the top view, e.g. to discriminate pixel movements or search for unusual motion patterns.



Algorithm 1 Image-based Top View Transformation

Require: Homography $W_{1...n}$, Camera Frames $I_{t,1...n}, I_{t-1,1...n}$, Background Frames $I_{bg,1...n}$
Ensure: Top view visualisation of pedestrian motion $I_{Topview}$
 $I_{Topview} \leftarrow 0$
for $i = 1$ to n **do**
 $I_{OF,i} \leftarrow \text{OpticalFlow}(I_{t,i}, I_{t-1,i})$
 $I_{Objects,i} \leftarrow \text{ImAbsDiff}(I_{t,i} - I_{BG,i})$
 $I_{Edges,i} \leftarrow \text{Edge}(I_{t,i}, \text{Canny})$
 $I_{MeanOF,i} \leftarrow \text{MeanOpticalFlow}(I_{Objects,i}, I_{OF,i})$
 $I_{Areas,i} \leftarrow \text{AngularThreshold}(I_{Edges,i}, I_{OF,i}, I_{Objects,i})$
 $I_{Topview} \leftarrow I_{Topview} + I_{Areas,i}$
 $W_{camToWorld,i}(I_{RemainingAreas,i})$
end for
 $I_{Topview} \leftarrow 1. * (I_{Topview} > n - 1)$

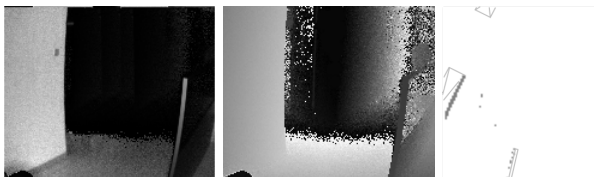


Fig. 3 Input footage from a calibrated Time-Of-Flight Sensor (intensity, left, depth value, middle) and a topview of the indoor scene captured by it (right).

and then proceed as described in Alg. 1. In the final step it uses the camera extrinsics and the depth values of interest, to project them onto xz -plane, the ground plane. This way, the intersection of pixel sets from several depth sensors with overlapping viewing cones is not necessary in the final step.

The altered algorithm is applied to the indoor sequence [27] captured with depth sensors as depicted in Table 2. The dataset both contains depth images and

Algorithm 2 Mean Optical Flow

Require: Connected Component Image $I_{Objects}$, Optical Flow Image I_{OF}
Ensure: Assignment of a mean flow vector for each connected component I_{MeanOF}
 $I_{MeanOF} \leftarrow 0$
for $i = 1$ to number of connected components in $I_{Objects}$ **do**
 $u_i \leftarrow 0, v_i \leftarrow 0$
 $counter \leftarrow 0$
 for each pixel p in $I_{Objects}$ and component i **do**
 $u_i \leftarrow u_i + u(p), v_i \leftarrow v_i + v(p)$
 $counter \leftarrow counter + 1$
 end for
 $u_i \leftarrow u_i / counter, v_i \leftarrow v_i / counter$
 for each pixel p in I_{MeanOF} and component i **do**
 [Assuming components of $I_{Objects}$]
 $u(p) \leftarrow u_i, v(p) \leftarrow v_i$
 $counter \leftarrow counter + 1$
 end for
end for

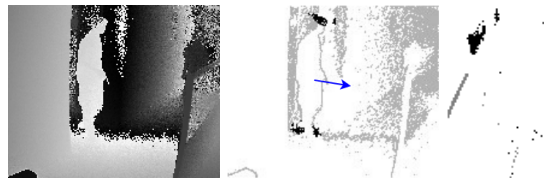
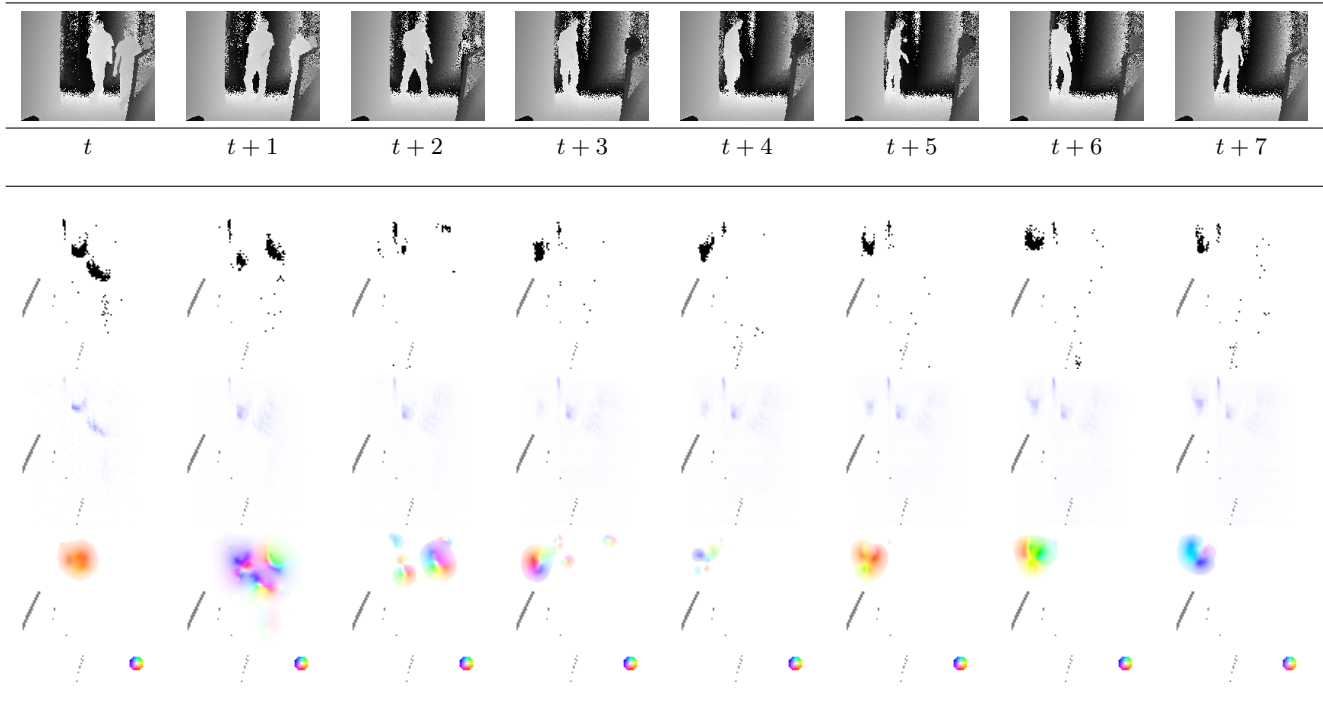


Fig. 4 A pedestrian captured by a Time-Of-Flight camera (first) is mapped to a top-view by finding edge segments colinear with the mean optical flow vector of the pedestrian (second) to get the overlay in the top view (third).

graylevel images. For our algorithm only used the depth images. The dataset was recorded with the Time-Of-Flight camera SwissRanger SR4000 from Mesa Imaging AG. Beside depth images, the camera can also cap-

Table 2 Analysis and summarization of an indoor pedestrian database [27]. The input data are captured with a Time-Of-Flight Camera.



Algorithm 3 AngularThreshold

Require: Edge Image I_{Edges} , Connected Component Image $I_{Objects}$, Optical Flow Image I_{OF}

Ensure: Assignment of remaining areas to be mapped to top view for each connected component I_{Areas}

```

 $I_{Areas} \leftarrow 0$ 
for  $i = 1$  to number of connected components in  $I_{Objects}$ 
do
  for each edge pixel  $p$  in  $I_{Edges}$  and component  $i$  do
     $dx(p) \leftarrow \frac{d}{dx} I_{Edges}$  at  $p$ 
     $dy(p) \leftarrow \frac{d}{dy} I_{Edges}$  at  $p$ 
    if  $(\text{atan2}(dy(p) - v(p), dx - u(p)) < \text{threshold})$  then
       $I_{Areas} \leftarrow 1$ 
    end if
  end for
  for each pixel  $p$  in  $I_{Areas}$  and component  $i$  do
    FloodFill in Line-Sweep Manner if there are two pixels  $p', p''$  with value 1 in the same horizontal line in  $I_{Areas}$ 
  end for
end for

```

ture synchronized intensity images. The resolutions of the depth images and intensity images are all 176 x 144 pixels and the distance was ranging from 0 to 5 meters. Using the TOF camera, 4637 pedestrian images and 198 non-pedestrian images in 3 different indoor environments have been captured. Pedestrians in these images are all standing or walking. The body orientation to the camera has not been limited and appear arbitrary in the sequences. A groundtruth dataset has been made available containing manually labeled pedestrian positions.

Algorithm 4 Depth-based Top View Transformation

Require: Camera Calibration matrix $C_{depthCam, 1 \dots n}$, Camera Frames $I_{t, 1 \dots n}, I_{t-1, 1 \dots n}$, Background Frames $I_{bg, 1 \dots n}$

Ensure: Top view visualisation of pedestrian motion

```

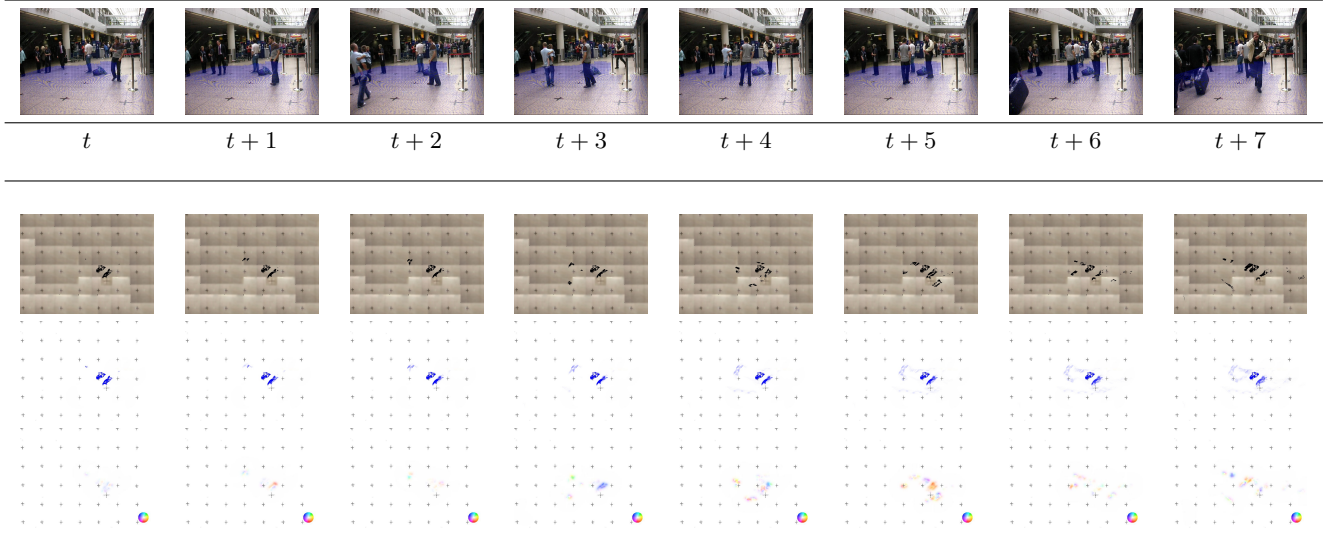
 $I_{Topview} \leftarrow 0$ 
 $I_{Topview} \leftarrow 0$ 
for  $i = 1$  to  $n$  do
   $I_{OF, i} \leftarrow \text{OpticalFlow}(I_{t, i}, I_{t-1, i})$ 
   $I_{Objects, i} \leftarrow \text{ImAbsDiff}(I_{t, i} - I_{BG, i})$ 
   $I_{Edges, i} \leftarrow \text{Edge}(I_{t, i}, \text{Canny})$ 
   $I_{MeanOF, i} \leftarrow \text{MeanOpticalFlow}(I_{Objects, i}, I_{OF, i})$ 
   $I_{Areas, i} \leftarrow \text{AngularThreshold}(I_{Edges, i}, I_{OF, i}, I_{Objects, i})$ 
  [Reproject Depth Values]
   $I_{Topview} \leftarrow I_{Topview} + C_{camToWorld, i}(I_{RemainingAreas, i}) \cdot (1, 0, 1)$ 
  [Discard Height Value]
end for
 $I_{Topview} \leftarrow 1 \cdot (I_{Topview} > n - 1)$ 

```

The 4637 pedestrian (positive) samples have originally been divided into two parts for training and testing purposes in pedestrian recognition: There are 3160 positive training samples, and 1477 positive test samples. Again, we apply the motion analysis by computing the cumulative grid, Table 2 third row, and the optical flow, Table 2 fourth row.

In a third example, RGB-Cameras are used in an indoor surveillance scenario, the capturing of pedestrian motion in a train station [1]. The calibration of the cameras has been conducted with Tsai's Algorithm by relying on equidistant markers that are placed on the floor of the

Table 3 Analysis and summarization of an indoor pedestrian database [1]. The crowding that is noticeable at time frames $t+2, t+3, t+4$ in the input images (first row) can be directly read from the cumulative top view scatterplot (third row). An optical flow computation can be applied to the top view, e.g. to discriminate pixel movements or search for unusual motion patterns.



terminal. The distance between the markers was 1.8m (to a tolerance of ± 1 cm). All spatial measurements have been set in metres, again. For recording, the following cameras were used: 2x Canon MV-1 1xCCD w/progressive scan, 2x Sony DCR-PC1000E 3xCMOS (full colour, 768 x 576 pixels, 25 frames per second). The video footage has been compressed as JPEG image sequences (approx. 90% quality). The dataset displays loitering behaviour (a person standing still for longer than 60 seconds), theft of belongings and leaving luggage behind. While the lighting conditions remained stable, the density of the crowd varied with each sequence. Its outcome is visualized in Table 3.

4 Results

We have applied the algorithm described in the previous section to all three datasets to retrieve cumulative grids and optical flow maps in the topview. The results for the PETS dataset 2009 [2] are listed in Table 4. In the S1 subsets the crowding behaviour is visible in the cumulative grid. In subset S2.L3 the positions of the two people who remain still throughout the sequence are imaged with saturated dots. In subset S3.MF the motion paths of the two people in yellow vests who approach the crowd are imaged as less saturated streaks.

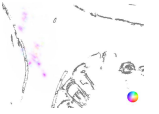
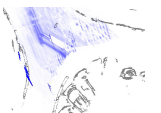
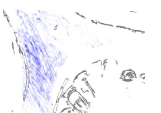
The results for the Depth Dataset [27] are listed in Table 5. In subset S16 the motion patterns of the three people are visible both in the cumulative grid and the optical flow map. The motion pattern of the three people moving far from the camera in subset S9 are well imaged in the optical flow map. The motion patterns

of two people crossing each other may confuse the optical flow algorithm, as seen in subset S1. The results for the PETS dataset 2007 [1] are listed in Table 6. Saturated spots indicate loitering people (S1) or bags which have been dropped (S2-S8). A streak towards the spot indicates suspicious behaviour, such as theft (S5). We have compared the performance of the algorithm on the datasets for a CPU and GPU implementation, Fig. 5. The algorithm has been implemented in C++ using the OpenCV library. The CPU code was run on a Intel i7 Dual Core Processor and GPU implementation was run on a NVIDIA GeForce GTX 690 with 2048Mb Cache, 1536 cores, and NVIDIA Driver 4.20. We compared the framerate in fps against the routine at idle, i.e. reading in the image streams without processing (*no operation*). It can be seen, that with the GPU implementation we can achieve real-time framerates (greater than 10 fps) that enable the pedestrian surveillance in top view with life cumulative maps. As all eight cameras were processed, the outdoor dataset [2] is the most consuming whereas the indoor depth dataset [27] with a single input stream is the least consuming.

5 Conclusion

We have presented an approach to retarget pedestrian surveillance footage into the topview in order to perform motion and video analysis to it. Two algorithms, one for RGB-data and one for depth data have been described in detail. The motion analysis consisted of cumulative maps to help crowding detection and the application of optical flows. We have applied the algorithm to an RGB outdoor

Table 4 The results of our algorithm applied to different sequences of the PETS dataset 2009 [2]

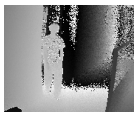
PETS dataset 2009 [2]	S1.L1	The sequence contains a medium density crowd, who are running. There are overcast lighting conditions				The cumulative grid shows the occupied area by the moving crowd in the middle of the sequence.
PETS dataset 2009 [2]	S1.L2	The sequence contains a high density crowd, who are walking in diverse directions. There are bright sunshine and shadows				The cumulative grid shows two blobs indicating the diversion of the flow.
PETS dataset 2009 [2]	S1.L3	The sequence contains a medium density crowd, who are walking. There are bright sunshine and shadows visible				The area occupied by the crowd is visible in the cumulative grid in the middle of the sequence.
PETS dataset 2009 [2]	S2.L1	The sequence contains a sparse crowd, who are walking. There are overcast lighting conditions visible				The cumulative grid is less dense. Few areas mainly traversed by the pedestrians appear more saturated in the grid.
PETS dataset 2009 [2]	S2.L2	The sequence contains a medium density crowd, who are walking. There are bright sunshine and shadows visible				The scattered incoherent crowd movements are visible in the less saturated grid.
PETS dataset 2009 [2]	S2.L3	The sequence contains a high density crowd, who are walking. There are overcast lighting conditions visible				In the grid, two saturated spots denote the position of the two men remaining still while the walking crowd is imaged in a less saturated region.
PETS dataset 2009 [2]	S3.HL	The sequence contains a high density crowd, who are running. There are bright sunshine and shadows visible				Three flows towards the scene center are recognisable in the cumulative grid and the flow map.
PETS dataset 2009 [2]	S3.MF	The sequence contains a high density crowd, who are performing different activities. There are overcast lighting conditions visible				Two disjunct streaks from the bottom to the top left of the grid indicate the paths of the men in yellow vest who are approaching the main crowd, which walks towards the scene centre.

dataset consisting of eight calibrated cameras and two indoor datasets. One dataset was a depth-based dataset consisting of one ToF-camera, the other was the surveillance of a train station with four extrinsically calibrated RGB cameras.

References

1. PETS 2007. Dataset of the tenth IEEE international workshop on performance evaluation of tracking and surveillance. <http://www.cvg.rdg.ac.uk/PETS2007/>.
2. PETS 2009. Dataset of the eleventh IEEE international workshop on performance evaluation of tracking and surveillance. <http://www.cvg.rdg.ac.uk/PETS2009/>.
3. A. Andriyenko, K. Schindler, and S. Roth. Discrete-continuous optimization for multi-target tracking.

Table 5 The results of our algorithm applied to different sequences of the Depth Dataset [27]

Depth Dataset [27]	S1	The sequence contains two people. One leaves the scene, one remains at his position.				The cumulative grid shows the trail of the one person moving from the scene and a blue saturated spot indicates that the other person remains still.
Depth Dataset [27]	S2	The sequence contains one person who is moving quickly away from the camera				The cumulative grid shows the trail of his body positions.
Depth Dataset [27]	S4	The sequence contains one person who is moving quickly parallel to the image plane				The cumulative grid shows the trail of his body positions.
Depth Dataset [27]	S6	The sequence contains two people. One moves away to the left, the other moves a bit to the camera				The cumulative grid shows the trail of both body positions.
Depth Dataset [27]	S9	The sequence contains three people. One vanishes to the rear right, one moves parallel to the image plane towards the right and one remains still				The cumulative grid shows the trail of all three body positions.
Depth Dataset [27]	S13	The sequence contains one person who slowly moves from the rear left towards the scene centre.				The slight faintest trail indicates the motion.
Depth Dataset [27]	S16	The sequence contains three people. One moves towards the camera, the second moves to the right, while the third remains still at the rear left.				The two trails are clearly visible, one spot indicates the person standing still.
Depth Dataset [27]	S19	The sequence contains one person who quickly moves towards the camera.				The less saturated trail indicates a fast paced motion.
Depth Dataset [27]	S22	The sequence contains one person who quickly moves from rear left to rear right.				The trail is visible in the upper part of the grid.

CVPR, 2012.

- Kai Berger, Kai Ruhl, Christian Brümmer, Yannic Schröder, Alexander Scholz, and Marcus Magnor. Markerless motion capture using multiple color-depth sensors. In *Proc. Vision, Modeling and Visualization (VMV)*, volume 2011, page 3, 2011.
- R. Borgo., M. Chen, B. Daubney, E. Grundy, H. Jaenicke, G. Heidemann, B. Hoferlin, M. Hoferlin, D. Weiskopf, and X. Xie. A survey on video-based graphics and video visualization. In *Eurographics 2011 STAR*, 2011.
- Ralf P. Botchen, Sven Bachthaler, Fabian Schick, Min Chen, Greg Mori, Daniel Weiskopf, and Thomas Ertl. Action-based multifield video visualization. 14(4):885–899, 2008.
- D Alex Butler, Shahram Izadi, Otmar Hilliges, David Molyneaux, Steve Hodges, and David Kim. Shake'n'sense: reducing interference for overlapping structured light depth cameras. In *Proceedings of the*

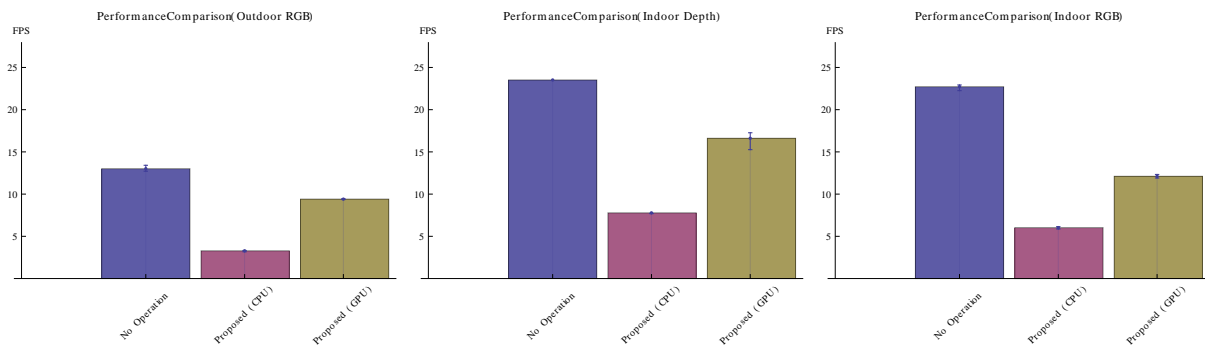
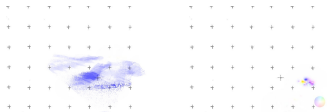


Fig. 5 The performance analysis for CPU vs. CUDA-accelerated implementations of the algorithm. We tested the algorithm with the three datasets. Since eight cameras have to be processed, the outdoor dataset [2] is the most consuming whereas the indoor depth dataset [27] with a single input stream is the least consuming. The GPU based implementation outperforms a purely CPU-based implementation and approximates an idle loop (no processing) more closely.

- 2012 ACM annual conference on Human Factors in Computing Systems, pages 1933–1936. ACM, 2012.
8. Robert Carroll, Aseem Agarwala, and Maneesh Agrawala. Image warps for artistic perspective manipulation. *ACM Trans. Graph.*, 29(4):127:1–127:9, July 2010.
 9. Min Chen, Ralf P. Botchen, Rudy R. Hashim, Daniel Weiskopf, Thomas Ertl, and Ian M. Thornton. Visual Signatures in Video Visualization. *IEEE Transactions on Visualization and Computer Graphics*, 12(5):1093–1100, 2006.
 10. Carlo Dal Mutto, Pietro Zanuttigh, and Guido Maria Cortelazzo. A probabilistic approach to tof and stereo data fusion. In *3DPVT*, Paris, France, May 2010.
 11. G.W. Daniel and M. Chen. Video visualization. *Proc. IEEE Visualization*, pages 409–416, October 2003.
 12. P Dollar, S Belongie, and P Perona. The fastest pedestrian detector in the west. *BMVC*, 2010.
 13. P Felzenszwalb, R Girshick, D McAllester, and D Ramanan. Object detection with discriminatively trained part-based models. *IEEE Trans. Pattern Anal. Mach. Intell.*, 2010.
 14. J. Fischer, G. Arbeiter, and A. Verl. Combination of time-of-flight depth and stereo using semiglobal optimization. In *Int. Conf. on Robotics and Automation (ICRA)*, pages 3548–3553. IEEE, 2011.
 15. Valentino Frati and Domenico Prattichizzo. Using kinect for hand tracking and rendering in wearable haptics. In *World Haptics Conference (WHC), 2011 IEEE*, pages 317–321. IEEE, 2011.
 16. Ross Girshick, Jamie Shotton, Pushmeet Kohli, Antonio Criminisi, and Andrew Fitzgibbon. Efficient regression of general-activity human poses from depth images. In *Computer Vision (ICCV), 2011 IEEE International Conference on*, pages 415–422. IEEE, 2011.
 17. H Gong, J Sim, M Likhachev, and J Shi. Multi-hypothesis motion planning for visual object tracking. *ICCV*, 2011.
 18. S.A. Gudmundsson, H. Aanaes, and R. Larsen. Fusion of stereo vision and time-of-flight imaging for improved 3d estimation. *IJISTA*, 5(3):425–433, 2008.
 19. U. Hahne and M. Alexa. Combining time-of-flight depth and stereo images without accurate extrinsic calibration. *IJISTA*, 5(3):325–333, 2008.
 20. U. Hahne and M. Alexa. Depth imaging by combining time-of-flight and on-demand stereo. *Dynamic 3D Imaging*, pages 70–83, 2009.
 21. Heiko Hirschmüller. Stereo processing by semiglobal matching and mutual information. *IEEE PAMI*, 30:328–341, 2008.
 22. C Huang, B Wu, and R Nevatia. Robust object tracking by hierarchical association of detection responses. *ECCV*, 2008.
 23. Y.M. Kim, C. Theobalt, J. Diebel, J. Kosecka, B. Miskusik, and S. Thrun. Multi-view image and tof sensor fusion for dense 3d reconstruction. In *ICCV Workshops*, pages 1542–1549. IEEE, 2009.
 24. K.D. Kuhnert and M. Stommel. Fusion of stereo-camera and pmd-camera data for real-time suited precise 3d environment reconstruction. In *Int. Conf. on Intelligent Robots and Systems*, pages 4780–4785. IEEE, 2006.
 25. P. Legg, M. Parry, D. Chung, R. Jiang, A. Morris, I. Griffiths, D. Marshall, and M. Chen. Intelligent filtering by semantic importance for single-view 3d reconstruction from snooker video. In *ICIP*, pages 2433–2436, 2011.
 26. Tommer Leyvand, Casey Meekhof, Yi-Chen Wei, Jian Sun, and Baining Guo. Kinect identity: Technology and experience. *Computer*, 44(4):94–96, 2011.
 27. Yan-Ran Li, Shiqi Yu, and Shengyin Wu. Pedestrian detection in depth images using framelet regularization. In *Computer Science and Automation Engineering (CSAE), 2012 IEEE International Conference on*, volume 2, pages 300–303. IEEE, 2012.
 28. Andrew Maimone and Henry Fuchs. Reducing interference multiple structured light depth sensors using motion. In *Virtual Reality Workshops (VR), 2012 IEEE*, pages 51–54. IEEE, 2012.
 29. Rahul Nair, Frank Lenzen, Stephan Meister, Henrik Schäfer, Christoph Garbe, and Daniel Kondermann. High accuracy tof and stereo sensor fusion at interactive rates. In *Computer Vision–ECCV 2012. Workshops and Demonstrations*, pages 1–11. Springer, 2012.
 30. Sebastian Nowozin, Carsten Rother, Shai Bagon, Toby Sharp, Bangpeng Yao, and Pushmeet Kohli. Decision tree fields. In *Computer Vision (ICCV), 2011 IEEE International Conference on*, pages 1668–1675. IEEE, 2011.
 31. Iason Oikonomidis, Nikolaos Kyriazis, and Antonis Argyros. Efficient model-based 3d tracking of hand articulations using kinect. *BMVC, Aug, 2*, 2011.
 32. T Parag, F Porikli, and A Elgammal. Boosting adaptive linear weak classifiers for online learning and tracking. *CVPR*, 2008.
 33. M. Parry, P. Legg, D. Chung, I. Griffiths, and M. Chen. Hierarchical event selection for video storyboards with a case study on snooker video visualization. In *IEEE Transactions on Visualization and Computer Graphics*, pages 1747–1756, 2011.
 34. H Pirsiavash, D Ramanan, and C Fowlkes. Globally-optimal greedy algorithms for tracking a variable number of objects. *CVPR*, 2011.

35. Jagdish L Raheja, Ankit Chaudhary, and Kunal Singal. Tracking of fingertips and centers of palm using kinect. In *Computational Intelligence, Modelling and Simulation (CIMSIM), 2011 Third International Conference on*, pages 248–252. IEEE, 2011.
36. Michalis Raptis, Darko Kirovski, and Hugues Hoppe. Real-time classification of dance gestures from skeleton animation. In *Proceedings of the 2011 ACM SIGGRAPH/Eurographics Symposium on Computer Animation*, pages 147–156. ACM, 2011.
37. M. Remero, J. Summet, J. Stasko, and G. Abowd. Viza-vis: Toward visualizing video through computer vision. *IEEE Transactions on Visualization and Computer Graphics*, 14(6):1261–1268, 2008.
38. M Rodriguez, I Laptev, J Sivic, and J Audibert. Density-aware person detection and tracking in crowds. *ICCV*, 2011.
39. L. Sacht, L. Velho, D. Nehab, and M. Cicconet. Scalable motion-aware panoramic videos. In *SIGGRAPH Asia 2011 Sketches*, page 37. ACM, 2011.
40. Yannic Schröder, Alexander Scholz, Kai Berger, Kai Ruhl, Stefan Guthe, and Marcus Magnor. Multiple kinect studies. *Computer Graphics*, 2011.
41. V. Setlur, S. Takagi, R. Raskar, M. Gleicher, and B. Gooch. Automatic image retargeting. In *Proceedings of the 4th international conference on Mobile and ubiquitous multimedia*, pages 59–68. ACM, 2005.
42. H Shitrit, J Berclaz, F Fleuret, and P. Fua. Tracking multiple people under global appearance constraints. *ICCV*, 2011.
43. Jamie Shotton, Andrew Fitzgibbon, Mat Cook, Toby Sharp, Mark Finocchio, Richard Moore, Alex Kipman, and Andrew Blake. Real-time human pose recognition in parts from single depth images. In *Computer Vision and Pattern Recognition (CVPR), 2011 IEEE Conference on*, pages 1297–1304. IEEE, 2011.
44. B Song, T Jeng, E Staudt, and A Roy-Chowdhury. A stochastic graph evolution framework for robust multi-target tracking. *ECCV*, 2010.
45. Michael Van den Bergh, Daniel Carton, Roderick De Nijs, Nikos Mitsou, Christian Landsiedel, Kolja Kuehnlentz, Dirk Wollherr, Luc Van Gool, and Martin Buss. Real-time 3d hand gesture interaction with a robot for understanding directions from humans. In *RO-MAN, 2011 IEEE*, pages 357–362. IEEE, 2011.
46. Yi Wang, D. M. Krum, E. M. Coelho, and D. A. Bowman. Contextualized videos: Combining videos with environment models to support situational understanding. *IEEE Transactions on Visualization and Computer Graphics*, 13(6):1568–1575, 2007.
47. M Yang, Y Wu, and G Hua. Context-aware visual tracking. *IEEE Trans. Pattern Anal. Mach. Intell.*, 2009.
48. Q. Yang, K.-H. Tan, B. Culbertson, and J. Apostolopoulos. Fusion of active and passive sensors for fast 3d capture. In *MMSP*, 2010.
49. J Yao and J Odobez. Multi-camera multi-person 3d space tracking with mcmc in surveillance scenarios. *ECCV, M2SFA2 Workshop*, 2008.
50. Michael Zollhöfer, Michael Martinek, Günther Greiner, Marc Stamminger, and Jochen Süßmuth. Automatic reconstruction of personalized avatars from 3d face scans. *Computer Animation and Virtual Worlds*, 22(2-3):195–202, 2011.

Table 6 The results of our algorithm applied to different sequences of the PETS dataset 2007 [1]

PETS dataset 2007 [1]	S1	The sequence contains one person who enters the scene and then loiters and leaves the scene.			In the cumulative grid with moving average $A_{t,t_{span}} = 100$ the position of the loitering person emerges visually.
PETS dataset 2007 [1]	S2	The sequence contains a person who walks into the scene and puts a bag on the ground. After loitering the person exits.			The loitering is visible in the cumulative map as blue saturated pixel set. The position of the bag becomes visible in the cumulative map from the moment of positioning until the end of the sequence.
PETS dataset 2007 [1]	S3	The sequence contains two people who enter the scene. One places a bag on the ground. The second person picks up the bag and both walk out.			Small saturated pixel regions in cumulative grid with moving average $A_{t,t_{span}} = 100$ indicate loitering of the two people. The optical flow map shows two spots diverging in different directions.
PETS dataset 2007 [1]	S4	The sequence contains four people who walk into the scene. One places a bag to the ground, another picks up the bag and all walk out of the scene.			The loitering is visible in the cumulative grid with moving average $A_{t,t_{span}} = 100$ as blue saturated pixel set.
PETS dataset 2007 [1]	S5	The sequence contains one person who the scene. They place the bag on the ground. A second person (thief) picks up the bag and walks out of the scene.			In the cumulative grid with moving average $A_{t,t_{span}} = 200$, the bag and the owner are visible as blob, with the more saturated pixel set showing the bag. The thief's approaching motion is seen in a less saturated second blob, that streaks towards the bag.
PETS dataset 2007 [1]	S6	The sequence contains two people. They place bags down on the ground. Two other people conduct theft and distraction.			Saturated blob in the cumulative grid with moving average $A_{t,t_{span}} = 300$ where the two people stand
PETS dataset 2007 [1]	S7	The sequence contains a single person with two bags. They place one bag on the ground, leave and return to pick up the left bag.			Saturated blob in the cumulative grid with moving average $A_{t,t_{span}} = 100$ where the person with the luggage stands.
PETS dataset 2007 [1]	S8	The sequence contains a person who places a large bag on the ground. He leaves the bag for a short moment before walking away with it.			Saturated blob in the cumulative grid with moving average $A_{t,t_{span}} = 100$ where the abandoned luggage lays.